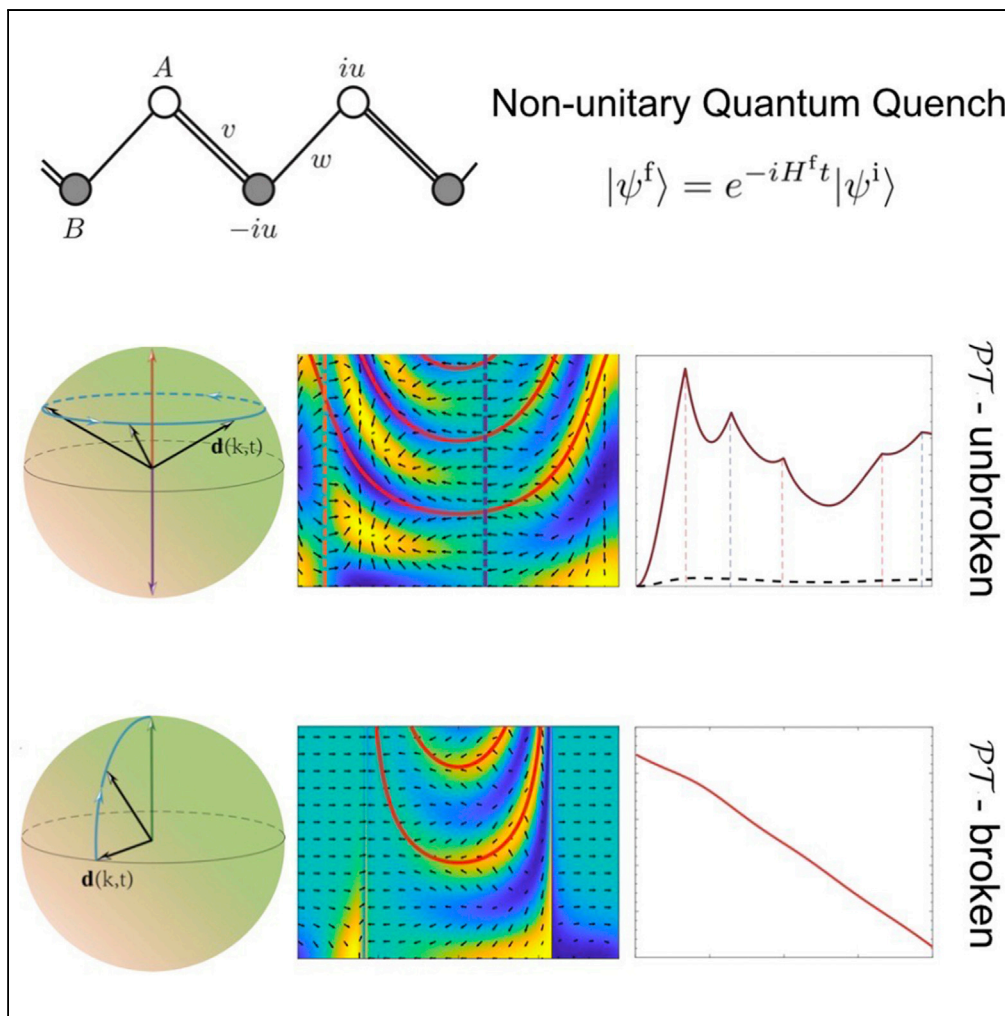


## Article

Fixed Points and Dynamic Topological Phenomena  
in a Parity-Time-Symmetric Quantum Quench

Xingze Qiu, Tian-Shu Deng, Ying Hu, Peng Xue, Wei Yi

huying@sxu.edu.cn (Y.H.)  
gnep.eux@gmail.com (P.X.)  
wyiz@ustc.edu.cn (W.Y.)

**HIGHLIGHTS**

Non-unitary quench dynamics of a PT-symmetric topological system

Fixed points exist for PT-symmetric quench between topologically distinct phases

Dynamic topological structures are constructed based on fixed points

Phenomena reported are readily detectable on synthetic quantum simulators

Qiu et al., iScience 20, 392–401  
October 25, 2019 © 2019 The Author(s).  
<https://doi.org/10.1016/j.isci.2019.09.037>



## Article

# Fixed Points and Dynamic Topological Phenomena in a Parity-Time-Symmetric Quantum Quench

Xingze Qiu,<sup>1,8</sup> Tian-Shu Deng,<sup>1,8</sup> Ying Hu,<sup>2,3,\*</sup> Peng Xue,<sup>4,5,6,\*</sup> and Wei Yi<sup>1,7,9,\*</sup>

## SUMMARY

We identify dynamic topological phenomena such as dynamic Chern numbers and dynamic quantum phase transitions in quantum quenches of the non-Hermitian Su-Schrieffer-Heeger Hamiltonian with parity-time ( $\mathcal{PT}$ ) symmetry. Their occurrences in the non-unitary dynamics are intimately connected with fixed points in the Brillouin zone, where the density matrices do not evolve in time. Based on our theoretical formalism characterizing topological properties of non-unitary dynamics, we prove the existence of fixed points for quenches between distinct static topological phases in the  $\mathcal{PT}$ -symmetry-preserving regime, thus unveiling the interplay between dynamic topological phenomena and  $\mathcal{PT}$  symmetry. Interestingly, non-Hermiticity of the driving Hamiltonian gives rise to rich dynamic topological phenomena which are different, either qualitatively or quantitatively, from their counterparts in unitary dynamics. Our work sheds light on dynamic topological phenomena in open systems and is readily accessible in experiments.

## INTRODUCTION

The exploration of topological matter constitutes a major theme in physics for the past few decades (Hasan and Kane, 2010; Qi and Zhang, 2011). With rapid progress in the discovery and understanding of topological phases in solid-state materials, a challenging quest lies in extending the study of conventional topological matter to unconventional regimes. Prominent examples include the investigation of dynamic topological properties in out-of-equilibrium dynamics (Budich and Heyl, 2016; Caio et al., 2015, 2016; Chang, 2018; D'Alessio and Rigol, 2015; Diehl et al., 2011; Eisert et al., 2015; Gong and Ueda, 2018; Heyl, 2015, 2018; Heyl et al., 2013; Hu et al., 2016; Huang and Balatsky, 2016; Jiang et al., 2011; Khemani et al., 2016; Kitagawa et al., 2010; Moessner and Sondhi, 2017; Potter et al., 2016; Rudner et al., 2013; Titum et al., 2016; Vajna and Dóra, 2015; Wang et al., 2017; Wilson et al., 2016; Yang et al., 2018; Zhang et al., 2019, 2018) and the characterization of topological phases in non-Hermitian systems (Deng and Yi, 2019; Esaki et al., 2011; Ghatak et al., 2019; Ghatak and Das, 2019; Gong et al., 2018; Helbig et al., 2019; Hofmann et al., 2019; Kawabata et al., 2018; Kim et al., 2016; Kunst et al., 2018; Lee and Thomale, 2019; Lee, 2016; Liang and Huang, 2013; Lieu, 2018; Martinez Alvarez et al., 2018; Rudner et al., 2016; Rudner and Levitov, 2009; Schomerus, 2013; Xiao et al., 2019; Yao et al., 2018; Yao and Wang, 2018; Yokomizo and Murakami, 2019; Zhou et al., 2018; Zhu et al., 2014). With the flexible controls afforded by synthetic systems such as ultracold atoms and engineered photonic configurations, the experimental implementation of these interesting scenarios is already within (Fläschner et al., 2016, 2018; Jotzu et al., 2014; Poli et al., 2015; Song et al., 2018; Tarnowski et al., 2019; Weimann et al., 2017; Xiao et al., 2017; Zeuner et al., 2015; Zhan et al., 2017).

An exemplary situation for the study of topological properties in out-of-equilibrium dynamics is the quantum quench of a topological system, where the ground state of the initial Hamiltonian  $H^i$  is subject to a unitary time evolution governed by the final Hamiltonian  $H^f$ . The topological invariant characterizing the instantaneous state is unchanged during the unitary dynamics (Caio et al., 2015; D'Alessio and Rigol, 2015), whereas previous studies have revealed the emergence of intriguing phenomena such as dynamic quantum phase transitions (DQPTs) (Budich and Heyl, 2016; Fläschner et al., 2018; Heyl, 2015, 2018; Heyl et al., 2013; Huang and Balatsky, 2016; Jurcevic et al., 2017; Vajna and Dóra, 2015) and quantized non-equilibrium Hall responses in quench processes (Caio et al., 2016; Hu et al., 2016; Wilson et al., 2016). Furthermore, in a series of recent theoretical and experimental studies, it has been established that dynamic topological invariants can be defined in unitary quantum quenches, which are related to the topology of initial and final Hamiltonians in equilibrium (Gong and Ueda, 2018; Tarnowski et al., 2019; Wang et al., 2017; Yang et al., 2018).

<sup>1</sup>CAS Key Laboratory of Quantum Information, University of Science and Technology of China, Hefei 230026, China

<sup>2</sup>State Key Laboratory of Quantum Optics and Quantum Optics Devices, Institute of Laser Spectroscopy, Shanxi University, Taiyuan, Shanxi 030006, China

<sup>3</sup>Collaborative Innovation Center of Extreme Optics, Shanxi University, Taiyuan, Shanxi 030006, China

<sup>4</sup>Beijing Computational Science Research Center, Beijing 100084, China

<sup>5</sup>Department of Physics, Southeast University, Nanjing 211189, China

<sup>6</sup>State Key Laboratory of Precision Spectroscopy, East China Normal University, Shanghai 200062, China

<sup>7</sup>CAS Center for Excellence in Quantum Information and Quantum Physics, Hefei 230026, China

<sup>8</sup>These authors contributed equally

<sup>9</sup>Lead Contact

\*Correspondence:  
huying@sxu.edu.cn (Y.H.),  
gnep.eux@gmail.com (P.X.),  
wyiz@ustc.edu.cn (W.Y.)

<https://doi.org/10.1016/j.isci.2019.09.037>



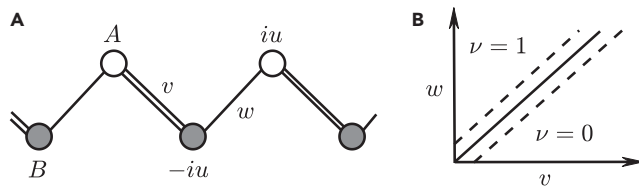


**Figure 1. Schematic illustration of the non-Hermitian SSH Hamiltonian and its phase diagram**

(A) Schematic illustration.

(B) Topological phase diagram. The solid line is the topological phase boundary with  $w = v$ . Dashed lines are the boundaries between  $PT$ -symmetry-preserving and broken regimes with  $|w-v| = u$ .

See also Figure S1.

Here arises a series of interesting questions: Are dynamic topological phenomena robust in open systems where dynamics is effectively driven by non-Hermitian Hamiltonians? How does one characterize dynamic topological phenomena in non-Hermitian/non-unitary settings? What new results would non-unitarity bring? These questions are particularly relevant in light of recent studies on topological phenomena in parity-time ( $PT$ )-symmetric non-Hermitian systems (El-Ganainy et al., 2018; Kawabata et al., 2018; Kim et al., 2016; Lieu, 2018; Özdemir et al., 2019; Poli et al., 2015; Schomerus, 2013; Weimann et al., 2017; Xiao et al., 2017; Zhu et al., 2014). Under  $PT$  symmetry, eigenenergies of a non-Hermitian Hamiltonian are entirely real in the  $PT$ -symmetry-preserving regime, in contrast to regimes with spontaneously broken  $PT$  symmetry (Bender, 2007; Bender and Boettcher, 1998; Bender et al., 2002). It has been shown that  $PT$  symmetry has profound impact on topological properties of static topological phases (Kawabata et al., 2018; Kim et al., 2016; Lieu, 2018; Poli et al., 2015; Schomerus, 2013; Weimann et al., 2017; Xiao et al., 2017; Zhu et al., 2014) and that the interplay of non-Hermiticity and dynamics in topological systems leads to non-trivial consequences (Rudner and Levitov, 2009; Zeuner et al., 2015; Zhan et al., 2017). However, the role of  $PT$  symmetry in dynamic topological phenomena associated with non-unitary dynamics has never been explored. A particular difficulty lies in the theoretical description of dynamics generated by non-Hermitian Hamiltonians, which is non-unitary even when the system is in the  $PT$ -symmetry-preserving regime with real eigen spectra. Searching for topological phenomena in dynamics of non-Hermitian systems thus requires theories beyond the conventional paradigm in Hermitian systems under unitary time evolution (D'Alessio and Rigol, 2015; Gong and Ueda, 2018; Tarnowski et al., 2019; Wang et al., 2017; Wilson et al., 2016; Yang et al., 2018).

In this work, we study the quench dynamics of a non-Hermitian Su-Schrieffer-Heeger (SSH) Hamiltonian with  $PT$  symmetry. We construct a general theoretical framework based on biorthogonal quantum mechanics, which is particularly suitable for characterizing dynamic topological properties in non-Hermitian systems. We then demonstrate that  $PT$  symmetry plays a key role in the robustness of dynamic topological phenomena, such as dynamic Chern numbers and DQPTs, under non-unitary dynamics. Importantly, these dynamic topological constructions exhibit both qualitative and quantitative differences from their counterparts in unitary dynamics: although the momentum-time submanifolds on which dynamic Chern numbers are defined undergo deformations, an additional timescale exists in the periodic occurrence of DQPTs, which necessitates the definition of two different dynamic topological order parameters. In both these cases, the underlying cause is traced back to fixed points in the non-unitary dynamics, which serve as building elements for the dynamic topological phenomena.

## RESULTS

### $PT$ -Symmetric SSH Model

As illustrated in Figure 1A, we consider the non-Hermitian SSH model with alternating gain and loss on adjacent sites under the periodic boundary condition (Lieu, 2018; Su et al., 1979):

$$H = \sum_{j=1}^{L-1} \left( v a_j^\dagger b_j + w a_{j+1}^\dagger b_j + \text{H.c.} \right) + iu \sum_{j=1}^L \left( a_j^\dagger a_j - b_j^\dagger b_j \right), \quad (\text{Equation 1})$$

where  $a_j^\dagger$  ( $b_j^\dagger$ ) is the creation operator on A (B) sub-lattice at site  $j$ ,  $L$  is the total number of unit cells, the tunneling amplitudes  $v, w$  and the gain-loss rate  $u$  satisfy  $u, v, w \geq 0$ , and H.c. stands for Hermitian conjugation. Note that without loss of generality, we assume  $u, v, w$  to be non-negative real numbers.

Hamiltonian (1) possess  $\mathcal{PT}$  symmetry, as  $\mathcal{PT}H(\mathcal{PT})^{-1} = H$ , with the parity operator  $\mathcal{P}a(b)_j\mathcal{P} = b(a)_{L+1-j}$ , and the time reversal operator  $\mathcal{T}i\mathcal{T}^{-1} = -i$ , respectively. Note that our definition of the parity operator relies on a cyclic indexing of unit cells such that an inversion center can be defined on the lattice despite the periodic boundary condition. Under  $\mathcal{PT}$  symmetry, the eigenspectrum of (1) is entirely real if all eigenstates are simultaneous eigenstates of the  $\mathcal{PT}$ -symmetry operator. In this case, the Hamiltonian is in the  $\mathcal{PT}$ -symmetry-preserving regime. Otherwise, the Hamiltonian is in the  $\mathcal{PT}$ -symmetry-broken regime, where some eigenstates spontaneously break  $\mathcal{PT}$  symmetry and acquire imaginary eigenenergies. The transition between the  $\mathcal{PT}$ -symmetry-preserving and broken regimes can be derived by examining the Bloch Hamiltonian  $H_k = \mathbf{h}(k) \cdot \boldsymbol{\sigma}$  at momentum  $k$ , where  $\boldsymbol{\sigma} = (\sigma_1, \sigma_2, \sigma_3)$  and  $\sigma_\alpha$  ( $\alpha = 1, 2, 3$ ) are the Pauli matrices. The complex vector  $\mathbf{h}(k) = (h_1, h_2, h_3)$ , with  $h_1 = w \cos k + v$ ,  $h_2 = w \sin k$ , and  $h_3 = iu$ . As the eigenenergy is given by  $\epsilon_\mu = \mu E_k$  ( $\mu = \pm$ ) with  $E_k = \sqrt{w^2 + v^2 + 2wv\cos k - u^2}$ , the Hamiltonian is in the  $\mathcal{PT}$ -symmetry-preserving regime when  $u < |v - w|$ , where  $\epsilon_\pm$  is real for all  $k$ .

The  $\mathcal{PT}$ -symmetric SSH Hamiltonian possesses topological properties, guaranteed by the so-called pseudo-anti-Hermiticity with  $\eta H^\dagger \eta^{-1} = -H$  (Esaki et al., 2011), where  $\eta = \sigma_z$ . As a result,  $\mathcal{PT}$ -symmetry-broken topological edge states with purely imaginary eigenenergies emerge at the boundary between bulks of different topological phases. Topologically inequivalent phases can be distinguished by the generalized winding number  $v = \varphi_B/2\pi$ . Here the global Berry phase  $\varphi_B$  is (Garrison and Wright, 1988; Liang and Huang, 2013; Lieu, 2018) (see Methods):

$$\varphi_B = -i \sum_{\mu=\pm} \oint dk \frac{\left\langle \chi_\mu \left| \frac{\partial}{\partial k} \right| \psi_\mu \right\rangle}{\langle \chi_\mu | \psi_\mu \rangle}, \quad (\text{Equation 2})$$

where the integral runs over the first Brillouin zone (1BZ) and the right (left) eigenvector is defined as  $H_k |\psi_\mu\rangle = \epsilon_\mu |\psi_\mu\rangle$  ( $H_k^\dagger |\chi_\mu\rangle = \epsilon_\mu^* |\chi_\mu\rangle$ ). When  $v < w$ , the system is topologically non-trivial, as  $v = 1$ . In contrast, when  $v > w$ , we have  $v = 0$  and the system is topologically trivial. In Figure 1B, we show the topological phase diagram as well as the boundary between  $\mathcal{PT}$ -symmetry-preserving and broken regimes. Notably, the  $\mathcal{PT}$ -symmetry-broken regime lies in the vicinity of the topological phase boundary.

Here an important remark is in order. In recent years, a general class of non-Hermitian topological models have been identified where the conventional bulk-boundary correspondence breaks down (Deng and Yi, 2019; Kunst et al., 2018; Lee and Thomale, 2019; Lee, 2016; Martinez Alvarez et al., 2018; Yao et al., 2018; Yao and Wang, 2018; Yokomizo and Murakami, 2019). Therein, topological invariants calculated from the homogeneous bulks fail to correctly predict topological edge states in a system with boundaries. Instead, one must invoke the definition of non-Bloch topological invariants, which take into account the localization (near system boundaries) of the bulk eigenstates under the non-Hermitian skin effect (Deng and Yi, 2019; Kunst et al., 2018; Lee and Thomale, 2019; Martinez Alvarez et al., 2018; Yao et al., 2018; Yao and Wang, 2018; Yokomizo and Murakami, 2019). However, since we focus on the quench dynamics of a homogeneous system without boundaries, it is sufficient that we only consider quantum quenches of the bulk Hamiltonian (1), where the parameters ( $u, v, w$ ) undergo abrupt changes at  $t = 0$ . Furthermore, we note that the non-Hermitian SSH model considered here does not suffer from non-Hermitian skin effects even in the presence of boundaries. For example, under the open-boundary condition, the bulk eigenstates are all extended and the Bloch topological invariant defined in Equation 2 is capable of correctly predicting topological edge states near the boundaries (see Figure S1 and Methods).

### Visualizing Non-unitary Dynamics on the Bloch Sphere

To account for the non-unitary dynamics of quenched non-Hermitian systems, we invoke the notion of biorthogonal quantum mechanics (Brody, 2013). Owing to the lattice translational symmetry of the Hamiltonian (1), dynamics in different  $k$ -sectors are decoupled and can be analyzed independently. Denoting the initial Hamiltonian by  $H^i$ , the initial state in each  $k$ -sector  $|\psi_-^i\rangle$ , with  $H_k^i |\psi_-^i\rangle = \epsilon_-^i |\psi_-^i\rangle$ , evolves under the final Hamiltonian  $H_k^f$  according to  $|\psi_k(t)\rangle = \sum_{\mu=\pm} c_\mu e^{-i\epsilon_\mu^f t} |\psi_\mu^f\rangle$ , where  $\epsilon_\mu^f = \mu E_k^f$  is the eigenenergy of  $H_k^f$ .

We have defined  $c_\mu = \langle \chi_\mu^f | \psi_-^i \rangle$ , where  $\langle \chi_\mu^f | (\psi_\mu^f) \rangle$  is the left (right) eigenvector of  $H_k^f$ , with the biorthonormal conditions  $\langle \chi_\mu^f | \psi_\nu^f \rangle = \delta_{\mu\nu}$  and  $\sum_\mu |\psi_\mu^f\rangle \langle \chi_\mu^f| = 1$ .

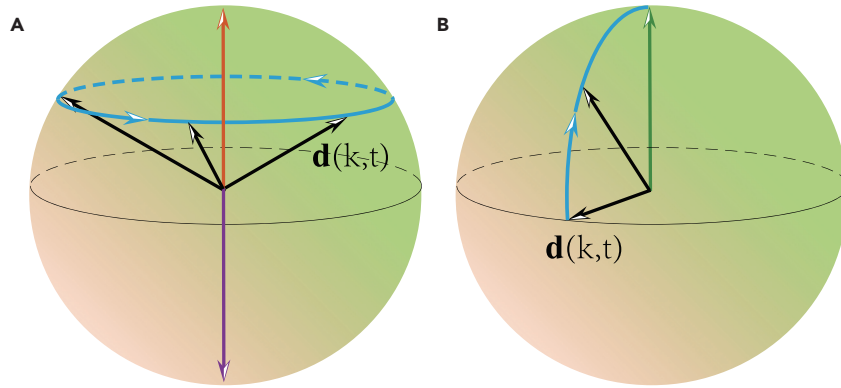


**Figure 2. Schematic Illustrations of the Time Evolution of  $d(k,t)$  on the Bloch Sphere**

Time evolution of  $d(k,t)$  (black) in  $k$ -sectors with: (A) real  $E_k^f$  and (B) imaginary  $E_k^f$  (assuming  $\text{Im}(E_k^f) > 0$ ). The orange and purple vectors correspond, respectively, to fixed points with  $c_- = 0$  and  $c_+ = 0$ . The green vector in (B) indicates the long-time steady state. See also Figure S2.

To characterize the non-unitary time evolution in the biorthogonal basis  $\{|\psi_\mu^f\rangle, |\chi_\mu^f\rangle\}$ , we define an associated state of  $|\psi_k(t)\rangle$  as  $\langle\chi_k(t)| = \sum_\mu c_\mu^* e^{iE_\mu^f t} \langle\chi_\mu^f|$  (Brody, 2013), with the normalization condition  $\langle\chi_k(0)|\psi_k(0)\rangle = 1$ .

The non-unitary time evolution of the system is then captured by the non-Hermitian density matrix  $\rho(k, t) = \frac{|\psi_k(t)\rangle\langle\chi_k(t)|}{\langle\chi_k(t)|\psi_k(t)\rangle}$ , such that the expectation value of any operator  $A_k$  is expressed as  $\text{Tr}(\rho A_k)$  (Brody, 2013). We further write

$$\rho(k, t) = \frac{1}{2}[\tau_0 + \mathbf{d}(k, t) \cdot \boldsymbol{\tau}], \quad (\text{Equation 3})$$

where  $\mathbf{d}(k, t) = (d_1, d_2, d_3)$ ,  $\boldsymbol{\tau} = (\tau_1, \tau_2, \tau_3)$ , and we have defined the matrices  $\tau_\gamma = \sum_{\mu, \nu= \pm} |\psi_\mu^f\rangle \sigma_\gamma^{\mu\nu} \langle\chi_\nu^f|$  ( $\gamma = 0, 1, 2, 3$ ).

Here  $\sigma_\gamma^{\mu\nu}$  is the matrix element of  $\sigma_\gamma$ , and  $\sigma_0$  is the  $2 \times 2$  identity matrix. Note that  $\{\tau_\gamma\}$  fulfill the standard  $\mathfrak{su}(2)$  algebra.

As a key ingredient of our theoretical construction, the choice of  $\rho(k, t)$  and the introduction of  $\{\tau_\gamma\}$  matrices make the corresponding  $\mathbf{d}(k, t)$  a real unit vector on the Bloch sphere  $S^2$ , even as the dynamics is non-unitary. Equation 3 thus allows a geometrical picture for understanding non-unitary dynamics and forms the basis for subsequent characterization of dynamic topological properties. Note that the non-Hermitian density matrix  $\rho(k, t)$  is connected to the conventional Hermitian one  $\rho'(k, t) = |\psi_k(t)\rangle\langle\psi_k(t)|$  through the metric operator  $g = \sum_\mu |\chi_\mu^f\rangle\langle\chi_\mu^f|$  (Brody, 2013), with  $\rho(k, t) = \frac{\rho'(k, t)g}{\text{Tr}[\rho'(k, t)g]}$  (Wang et al., 2019a). Although either density matrix can be used for the characterization of dynamic topological phenomena (Wang et al., 2019a), it is formally more elegant and convenient to use  $\rho(k, t)$  (see Methods), not the least because it is then straightforward to visualize non-unitary dynamics on the Bloch sphere.

### Fixed Points in Non-unitary Dynamics

When  $E_k^f$  is real,  $\mathbf{d}(k, t)$  and hence the density matrix  $\rho(k, t)$  are oscillatory in time, with a momentum-dependent period  $t_0 = \pi/E_k^f$  (see Methods). This corresponds to a periodic rotation of  $\mathbf{d}(k, t)$  around the poles of the Bloch sphere, as illustrated in Figure 2A. Importantly, when  $\mathbf{d}(k, 0)$  is on the poles of the Bloch sphere, the density matrix becomes time independent. This occurs at momenta  $k_m$  with either  $c_-(k_m) = 0$  (north pole) or  $c_+(k_m) = 0$  (south pole), which are identified as two different kinds of fixed points. In contrast, when  $E_k^f$  is imaginary,  $\mathbf{d}(k, t)$  always starts from the equator at  $t = 0$  and approaches the north pole in the long-time limit (Figure 2B), i.e.,  $\rho(k, t)$  exponentially approaches a steady-state value (see Methods). In this case, there are no fixed points in the dynamics. Detailed time evolutions of  $\mathbf{d}(k, t)$  under different parameters are shown in Figure S2.

Based on the aforementioned understanding, it is straightforward to show that the number of fixed points with  $c_+ = 0$  or  $c_- = 0$  should be at least  $|\nu^i - \nu^f|$  each, provided both  $H^i$  and  $H^f$  belong to the  $\mathcal{PT}$ -symmetry-preserving

regime with completely real eigenspectra (see [Methods](#)). Here  $\nu^\beta$  ( $\beta = i, f$ ) are the generalized winding numbers of  $H^\beta$ . On the other hand, when  $H^f$  is in the  $\mathcal{PT}$ -symmetry-broken regime, the corresponding  $E_k^f$  becomes imaginary for a certain range of  $k$ , and the existence of fixed points are no longer guaranteed. We note that, although in the unitary limit ( $u=0$ ), our conclusions agree with previous studies ([Gong and Ueda, 2018; Yang et al., 2018](#)), our theoretical formalism is quite different from previous cases even for unitary dynamics. This is because matrices  $\tau_\gamma$  are not reduced to Pauli matrices for  $u=0$ , such that our mapping from quantum-state dynamics to the Bloch sphere is different from previous studies. It is also worth mentioning that, when starting from the Hermitian density matrix  $\rho'(k, t)$ , it becomes quite difficult to theoretically relate the number and type of fixed points to the static topological invariants of the non-Hermitian Hamiltonians.

In the following, we mainly focus on the case where both  $H^i$  and  $H^f$  are in the  $\mathcal{PT}$ -symmetry-preserving regime. When the system is quenched across the topological phase boundary, fixed points divide the BZ into a series of submanifolds, where the density matrices at two ends of each given submanifold do not evolve in time. Fixed points in non-unitary dynamics are protected by both  $\mathcal{PT}$  symmetry and band topology of the pre- and post-quench Hamiltonians, as we detail in the remainder of the work, whereas their physical consequences are manifested as observable dynamic topological phenomena such as dynamic skyrmions and DQPTs.

### Dynamic Chern Number

When  $H^f$  is in the  $\mathcal{PT}$ -symmetry-preserving regime, the periodic oscillation of the density-matrix evolution gives rise to an  $S^1$  topology in the time evolution. In the presence of fixed points, each submanifold between two adjacent fixed points can be combined with the  $S^1$  topology in time to form a momentum-time manifold  $S^2$ , which can be mapped to the Bloch sphere associated with the vector  $d(k, t)$  ([Gong and Ueda, 2018; Yang et al., 2018](#)). These  $S^2 \rightarrow S^2$  mappings define a series of dynamic Chern numbers

$$C_{mn} = \frac{1}{4\pi} \int_{k_m}^{k_n} dk \int_0^{t_0} dt [d(k, t) \times \partial_t d(k, t)] \cdot \partial_k d(k, t), \quad (\text{Equation 4})$$

where  $k_m$  and  $k_n$  denote two neighboring fixed points. For quenches between Hamiltonians with different winding numbers, the dynamic Chern numbers are quantized, with values dependent on the nature of fixed points at  $k_m$  and  $k_n$  (see [Methods](#)):  $C_{mn} = 1$  when  $c_+(k_m) = 0$  and  $c_-(k_n) = 0$ ;  $C_{mn} = -1$  when  $c_-(k_m) = 0$  and  $c_+(k_n) = 0$ . When the two fixed points are of the same kind,  $C_{mn} = 0$ .

The emergence of finite dynamic Chern numbers can be visualized in the spin textures of  $d(k, t)$ , which possess skyrmion-lattice structures in the momentum-time space ([Gong and Ueda, 2018; Skyrme, 1962](#)), with the skyrmion number equivalent to the dynamic Chern number in each  $S^2$  momentum-time submanifold. In [Figure 3](#), we show these skyrmion-lattice structures for different quench parameters. When the system is quenched across the topological phase boundary with  $|\nu^i - \nu^f| = 1$ , as we illustrate in [Figures 3A and 3B](#), two fixed points of different kinds exist in the BZ. In the unitary limit ([Figure 3A](#)), the fixed points are pinned at  $k = 0$  and  $\pi$  ([Gong and Ueda, 2018; Yang et al., 2018](#)). In the more general non-unitary case ([Figure 3B](#)), fixed points deviate from 0 and  $\pi$  and need to be solved from  $c_\pm(k_m) = 0$ . Pairs of vortices with positive (yellow) or negative (blue) vorticity emerge in the spin texture between adjacent fixed points on the plane of  $d_1-d_3$ , with vortex cores given by  $d_2(k, t) = \pm 1$ . These vortices can be mapped to a lattice of skyrmions, whose topological charges are essentially the dynamic Chern numbers. In contrast, skyrmions are absent when  $H^i$  and  $H^f$  belong to the same topological phase ([Figure 3C](#)).

For comparison, in [Figure 3D](#), we plot the spin texture when  $H^f$  is in the  $\mathcal{PT}$ -symmetry-broken regime. As expected, in the momentum range where  $E_k^f$  is imaginary, the spin texture approaches a steady state in the long-time limit, in sharp contrast to the periodic spin dynamics in the momentum range with real  $E_k^f$ . We note that coincidental fixed points may still exist in the momentum range where  $E_k^f$  is real (see [Figure S3](#) and [Methods](#)), but their number is no longer directly related to the topology of  $H^i$  and  $H^f$ .

### Dynamic Quantum Phase Transition

Fixed points in the non-unitary quench dynamics further give rise to DQPTs, where physical quantities become nonanalytic at critical times. Interestingly, we find that, although DQPTs occur biperiodically in time for non-unitary quench dynamics, critical points of DQPTs generically emerge as vortex cores in the momentum-time-space spin texture, which provides a crucial link between different dynamic topological phenomena.

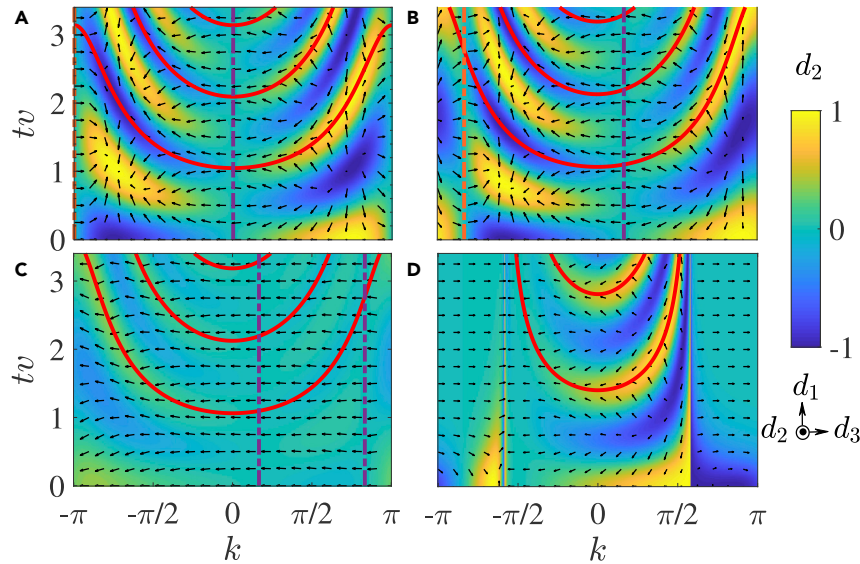


**Figure 3. Dynamics of Spin Textures  $d(k,t)$  in the  $k\text{-}t$  Space**

Quench processes are between  $H^i$  and  $H^f$  characterized by: (A) ( $u^i = 0, w^i = v/3$ ) and ( $u^f = 0, w^f = 2v$ ); (B) ( $u^i = v/2, w^i = v/3$ ) and ( $u^f = v/2, w^f = 2v$ ); (C) ( $u^i = v/2, w^i = 3v$ ) and ( $u^f = v/2, w^f = 2v$ ); (D) ( $u^i = v/2, w^i = v/3$ ) and ( $u^f = 2v, w^f = 2v$ ). We fix  $v^i = v^f = v$  in the quenches, whereas the dynamic is unitary in (A) and non-unitary in (B–D). The vertical dash-dotted lines in (A)–(C) indicate fixed points with  $c_+ = 0$  (purple) and  $c_- = 0$  (orange), respectively. Skyrmion lattices associated with finite dynamic Chern numbers only emerge in (A) and (B). The solid red lines in the horizontal direction mark each period  $n\pi/E_k^f$  ( $n = 1, 2, \dots$ ) of spin oscillation in regions with real  $E_k^f$ . The spin dynamics is non-oscillatory in regions with imaginary  $E_k^f$ , as shown in (D). The color bar indicates the value of  $d_2$ , while the arrows indicate the spin texture in the  $d_1\text{-}d_2$  plane. See also Figure S3.

The central object in the theory of DQPT is the Loschmidt amplitude defined as the inner product of a time-evolved state with the initial state (Heyl, 2018). In non-unitary time evolutions, we generalize the Loschmidt amplitude as:

$$\mathcal{G}(t) = \prod_{k \in 1\text{BZ}} \mathcal{G}_k(t) = \prod_{k \in 1\text{BZ}} \langle \chi_k(0) | \psi_k(t) \rangle, \quad (\text{Equation 5})$$

where  $\langle \chi_k(t) |$  is the associated state of  $|\psi_k(t)\rangle$  defined previously. It is straightforward to derive  $\mathcal{G}_k(t) = |c_-|^2 e^{iE_k^f t} + |c_+|^2 e^{-iE_k^f t}$ .

DQPTs occur when the rate function  $g(t) = -\frac{1}{L} \ln(|\mathcal{G}(t)|^2)$  exhibits nonanalyticities during the time evolution, which are caused by Fisher zeros (Heyl, 2018), where  $\mathcal{G}_{k_c}(t_c) = 0$  at critical points  $k_c$  and  $t_c$  in the dynamics. According to the expression of  $\mathcal{G}_k(t)$ , Fisher zeros, and hence DQPTs, occur periodically at  $t_c = \left(n + \frac{1}{2}\right)\pi/E_{k_c}^f$  ( $n \in \mathbb{N}$ ) when  $E_{k_c}^f$  is real. Here  $k_c$  satisfies  $|c_-(k_c)| = |c_+(k_c)|$ . When the system is quenched between different topological phases in the  $\mathcal{PT}$ -symmetry-preserving regime, fixed points with  $c_+ = 0$  and those with  $c_- = 0$  always emerge in pairs. As  $|c_+| - |c_-|$  are continuous functions of  $k$ , there must be at least one critical momentum satisfying  $|c_+(k_c)| = |c_-(k_c)|$  between two fixed points of different kinds. We thus conclude that DQPTs necessarily occur in this case.

Interestingly, at critical points,  $d_2(k_c, t_c) = 1$ , which lie on the equator of the Bloch sphere (see Methods). The critical points  $(k_c, t_c)$  thus correspond to vortex cores with positive vorticity in the momentum-time spin texture (Figures 3A and 3B). As vortices are manifestations of skyrmions, whose topological charges are the dynamic Chern numbers, the dynamic topological phenomena are related through the spin texture.

DQPTs are characterized by the dynamic topological order parameter  $\nu_D$ , which is defined through the Pancharatnam geometric phase (PGP)  $\phi_k^G(t)$  as:

$$\nu_D(t) = \frac{1}{2\pi} \int_{k_m}^{k_p} \frac{\partial \phi_k^G(t)}{\partial k} dk. \quad (\text{Equation 6})$$

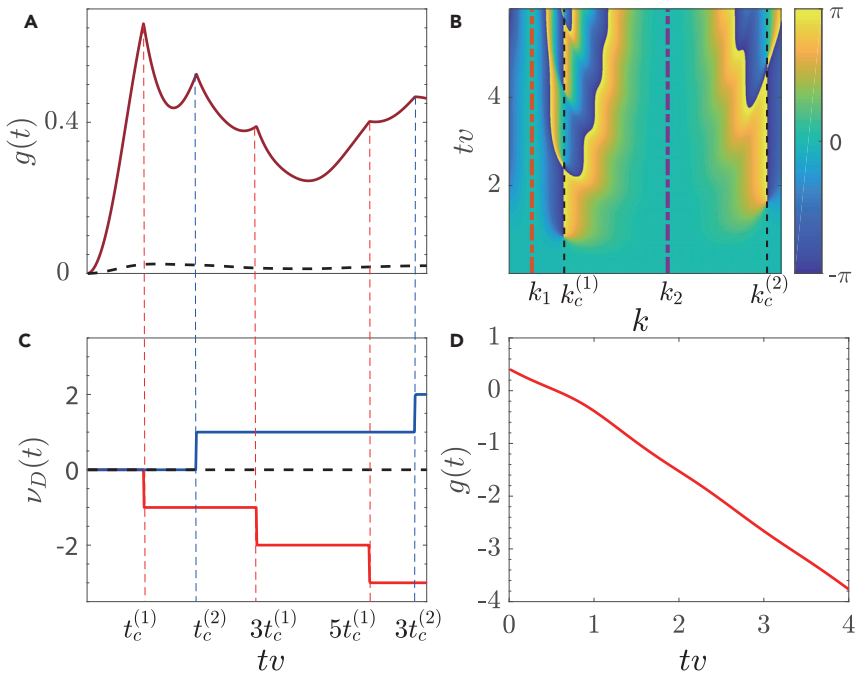


**Figure 4. DQPTs and Dynamic Topological Order Parameters in Non-Unitary Quench Dynamics**

(A) The rate function  $g(t)$ , (B) the PGP  $\phi_k^G(t)$ , and (C) the dynamic topological order parameter  $\nu_D$  for the quench in Figure 3B. At fixed points  $k_m$  ( $m = 1, 2$ ),  $c_-(k_1) = 0$ , and  $c_+(k_2) = 0$ .  $k_c^{(m)}$  and  $t_c^{(m)} = \pi/(2E_{k_c^{(m)}}^f)$  are the corresponding critical points. Two distinct types of  $\nu_D(t)$  exist in (C), obtained by setting the range of integral in Equation 6 as  $(k_1, k_2)$  (red) and  $(k_2, k_1+2\pi)$  (blue), respectively. The black dashed lines in (A) and (C) correspond to the quench in Figure 3C, whereas the quench in (D) is the same as that in Figure 3D. The color bar in (B) indicates the value of PGP. See also Figure S3.

Here,  $k_m$  and  $k_n$  are fixed points of different kinds, and  $\phi_k^G(t) = \phi_k(t) - \phi_k^{\text{dyn}}(t)$ , where  $\phi_k(t)$  is defined through  $\mathcal{G}_k(t) = |\mathcal{G}_k(t)|e^{i\phi_k(t)}$  and the dynamic phase  $\phi_k^{\text{dyn}}(t) = -\int_0^t \langle \chi_k(t') | H_k^f | \psi_k(t') \rangle dt'$ . At critical points,  $\mathcal{G}_k(t)$  vanishes, which leads to abrupt jumps in  $\phi_k^G(t)$  and  $\nu_D(t)$ . Furthermore, as  $\phi_k^G(t)$  also vanishes at fixed points,  $\nu_D$  characterizes the  $S^1 \rightarrow S^1$  mapping from the momentum submanifold between  $k_m$  and  $k_n$  to  $e^{i\phi_k^G(t)}$  on the same momentum submanifold.  $\nu_D(t)$  is therefore quantized despite the non-unitary time evolution.

In Figures 4A–4C, we show typical  $g(t)$ ,  $\phi_k^G(t)$ , and  $\nu_D(t)$  for a quench between different topological phases in the  $\mathcal{PT}$ -symmetry-preserving regime. The BZ is divided into two submanifolds by the fixed points  $k_1$  and  $k_2$ , where each submanifold contains a critical momentum, labeled as  $k_c^{(1)}$  and  $k_c^{(2)}$ , respectively. These critical momenta give rise to two distinct critical time scales  $t_c^{(1)}$  and  $t_c^{(2)}$ , and thus an apparent biperiodicity in the occurrence of DQPTs (Figure 4A), in contrast to its single-period counterpart in the unitary limit ( $u = 0$ ) (Heyl, 2015, 2018). This is due to the breaking of time reversal symmetry under the non-Hermitian SSH Hamiltonian (1), such that the double degeneracy of Fisher zeros in the Hermitian case is lifted (Vajna and Dóra, 2015). Correspondingly, two distinct types of  $\nu_D(t)$  exist, accounting for DQPTs occurring with the period  $t_c^{(1)}$  and  $t_c^{(2)}$ , respectively (Figure 4C). In contrast, when  $H^i$  and  $H^f$  have the same winding numbers,  $g(t)$  is a smooth function in time and  $\nu_D(t) = 0$  (dashed lines in Figures 4A and 4C).

Finally, when  $H^f$  is in the  $\mathcal{PT}$ -symmetry-broken regime, DQPT is not guaranteed (see Figure S3 and Methods), even if  $H^i$  and  $H^f$  possess different winding numbers. In Figure 4D, we demonstrate the typical rate function  $g(t)$  for the quench process in Figure 3D, where neither fixed points nor DQPTs are present.

## DISCUSSION

We have shown that dynamic topological phenomena emerge in the quench dynamics of a  $\mathcal{PT}$ -symmetric non-Hermitian SSH model. These dynamic topological phenomena are connected with discrete fixed points in the post-quench dynamics and emerge in the non-unitary time evolution when the system is quenched between different topological phases in  $\mathcal{PT}$ -symmetry-preserving regime. Given the recent experimental observation of spontaneous  $\mathcal{PT}$ -symmetry breaking in cold atoms (Li et al., 2019) and

topological edge states in  $\mathcal{PT}$ -symmetric quantum-walk dynamics (Xiao et al., 2017), we expect that the dynamic topological phenomena discussed here can be probed using cold atoms loaded into a superlattice with engineered on-site loss, or through discrete-time quantum-walk dynamics in photonic configurations (Wang et al., 2019a, 2019b). For either the cold atom or the photonic setup, tomography of instantaneous time-evolved states is needed to probe the dynamic topological phenomena.

### Limitations of the Study

In this study, we only consider quench dynamics of a homogeneous, non-interacting SSH model with on-site gain and loss. The results obtained, namely, the presence of fixed points and the appearance of dynamic topological structures, may be different, either quantitatively or qualitatively, in a different setting. For example, the fate of the dynamic topological phenomena is unknown for systems with boundaries, or with interactions. Neither is the presence of fixed points and dynamic topological structures entirely clear for systems with different topological classifications, or with alternative forms of non-Hermiticity. We leave these unaddressed questions to future studies.

### METHODS

All methods can be found in the accompanying [Transparent Methods supplemental file](#).

### SUPPLEMENTAL INFORMATION

Supplemental Information can be found online at <https://doi.org/10.1016/j.isci.2019.09.037>.

### ACKNOWLEDGMENT

This work has been supported by the National Natural Science Foundation of China (Grant Nos. 11434007, 11474049, 11674056, 11522545, 11874038 and U1930402), the National Key Research and Development Program of China (Grant Nos. 2016YFA0301700, 2017YFA0304203), Changjiang Scholars and Innovative Research Team in University of Ministry of Education of China (Grant No. IRT13076), and the Natural Science Foundation of Jiangsu Province (Grant No. BK20160024). Y. H. also acknowledges support from the National Thousand-Young-Talents Program, and Shanxi 100 Talents Program.

### AUTHOR CONTRIBUTIONS

W.Y., Y.H., and P.X. conceived the project; X.Q. and T.-S.D. performed the theoretical analysis; W.Y., Y.H., and P.X. wrote the paper with input from other authors. All authors contributed to revising the paper.

### DECLARATION OF INTERESTS

The authors declare no competing interests.

Received: July 1, 2019

Revised: August 23, 2019

Accepted: September 24, 2019

Published: October 25, 2019

### REFERENCES

- Bender, C.M. (2007). Making sense of non-Hermitian Hamiltonians. *Rep. Prog. Phys.* *70*, 947.
- Bender, C.M., and Boettcher, S. (1998). Real spectra in non-Hermitian Hamiltonians having  $\mathcal{PT}$  symmetry. *Phys. Rev. Lett.* *80*, 5243.
- Bender, C.M., Brody, D.C., and Jones, H.F. (2002). Complex extension of quantum mechanics. *Phys. Rev. Lett.* *89*, 270401.
- Brody, D.C. (2013). Biorthogonal quantum mechanics. *J. Phys. A Math. Theor.* *47*, 035305.
- Budich, J.C., and Heyl, M. (2016). Dynamical topological order parameters far from equilibrium. *Phys. Rev. B* *93*, 085416.
- Caio, M.D., Cooper, N.R., and Bhaseen, M.J. (2015). Quantum quenches in Chern insulators. *Phys. Rev. Lett.* *115*, 236403.
- Caio, M.D., Cooper, N.R., and Bhaseen, M.J. (2016). Hall response and edge current dynamics in Chern insulators out of equilibrium. *Phys. Rev. B* *94*, 155104.
- Chang, P.-Y. (2018). Topology and entanglement in quench dynamics. *Phys. Rev. B* *97*, 224304.
- D'Alessio, L., and Rigol, M. (2015). Dynamical preparation of floquet chern insulators. *Nat. Commun.* *6*, 8336.
- Deng, T.-S., and Yi, W. (2019). Non-bloch topological invariants in a non-Hermitian domain-wall system. *Phys. Rev. B* *100*, 035102.
- Diehl, S., Rico, E., Baranov, M.A., and Zoller, P. (2011). Topology by dissipation in atomic quantum wires. *Nat. Phys.* *7*, 971–977.
- Eisert, J., Friesdorf, M., and Gogolin, C. (2015). Quantum many-body systems out of equilibrium. *Nat. Phys.* *11*, 124–130.
- El-Ganainy, R., Makris, K.G., Khajavikhan, M., Musslimani, Z.H., Rotter, S., and Christodoulides, D.N. (2018). Non-Hermitian physics and  $\mathcal{PT}$  symmetry. *Nat. Phys.* *14*, 11–19.

- Esaki, K., Sato, M., Hasebe, K., and Kohmoto, M. (2011). Edge states and topological phases in non-Hermitian systems. *Phys. Rev. B* 84, 205128.
- Fläschner, N., Rem, B.S., Tarnowski, M., Vogel, D., Lühmann, D.-S., Sengstock, K., and Weitenberg, C. (2016). Experimental reconstruction of the Berry curvature in a floquet bloch band. *Science* 352, 1091–1094.
- Fläschner, N., Vogel, D., Tarnowski, M., Rem, B.S., Lühmann, D.-S., Heyl, M., Budich, J.C., Mathey, L., Sengstock, K., and Weitenberg, C. (2018). Observation of dynamical vortices after quenches in a system with topology. *Nat. Phys.* 14, 265.
- Garrison, J.C., and Wright, E.M. (1988). Complex geometrical phases for dissipative systems. *Phys. Lett. A* 128, 177–181.
- Ghatak, A., Brandenburger, M., van Wezel, J., and Coulais, C. (2019). Observation of non-Hermitian topology and its bulk-edge correspondence. *arXiv*, 1907.11619.
- Ghatak, A., and Das, T. (2019). New topological invariants in non-Hermitian systems. *J. Phys. Condens. Matter.* 31, 263001.
- Gong, Z., Ashida, Y., Kawabata, K., Takasan, K., Higashikawa, S., and Ueda, M. (2018). Topological phases of non-Hermitian systems. *Phys. Rev. X* 8, 031079.
- Gong, Z., and Ueda, M. (2018). Topological entanglement-spectrum crossing in quench dynamics. *Phys. Rev. Lett.* 121, 250601.
- Hasan, M.Z., and Kane, C.L. (2010). Colloquium: topological insulators. *Rev. Mod. Phys.* 82, 3045.
- Helbig, T., Hofmann, T., Imhof, S., Abdelghany, M., Kiessling, T., Molenkamp, L.W., Lee, C.H., Szameit, A., Greiter, M., and Thomale, R. (2019). Observation of bulk boundary correspondence breakdown in topolectrical circuits. *arXiv*, 1907.11562.
- Heyl, M. (2015). Scaling and universality at dynamical quantum phase transitions. *Phys. Rev. Lett.* 115, 140602.
- Heyl, M. (2018). Dynamical quantum phase transitions: a review. *Rep. Prog. Phys.* 81, 054001.
- Heyl, M., Polkovnikov, A., and Kehrein, S. (2013). Dynamical quantum phase transitions in the transverse-field Ising model. *Phys. Rev. Lett.* 110, 135704.
- Hofmann, T., Helbig, T., Schindler, F., Salgo, N., Brzezińska, M., Greiter, M., Kiessling, T., Wolf, D., Vollhardt, A., Kabaśi, A., et al. (2019). Reciprocal skin effect and its realization in a topolectrical circuit. *arXiv*, 1908.02759.
- Hu, Y., Zoller, P., and Budich, J.C. (2016). Dynamical buildup of a quantized Hall response from nontopological states. *Phys. Rev. Lett.* 117, 126803.
- Huang, Z., and Balatsky, A.V. (2016). Dynamical quantum phase transitions: role of topological nodes in wave function overlaps. *Phys. Rev. Lett.* 117, 086802.
- Jiang, L., Kitagawa, T., Alicea, J., Akhmerov, A.R., Pekker, D., Refael, G., Cirac, J.I., Demler, E., Lukin, M.D., and Zoller, P. (2011). Majorana fermions in equilibrium and in driven cold-atom quantum wires. *Phys. Rev. Lett.* 106, 220402.
- Jotzu, G., Messer, M., Desbuquois, R., Lebrat, M., Uehlinger, T., Greif, D., and Esslinger, T. (2014). Experimental realization of the topological Haldane model with ultracold fermions. *Nature* 515, 237–240.
- Jurcevic, P., Shen, H., Hauke, P., Maier, C., Brydges, T., Hempel, C., Lanyon, B.P., Heyl, M., Blatt, R., and Roos, C.F. (2017). Direct observation of dynamical quantum phase transitions in an interacting many-body system. *Phys. Rev. Lett.* 119, 080501.
- Kawabata, K., Ashida, Y., Katsura, H., and Ueda, M. (2018). Parity-time-symmetric topological superconductor. *Phys. Rev. B* 98, 085116.
- Khemani, V., Lazarides, A., Moessner, R., and Sondhi, S.L. (2016). Phase structure of driven quantum systems. *Phys. Rev. Lett.* 116, 250401.
- Kim, D., Ken, M., Kawakami, N., and Obuse, H. (2016). Floquet topological phases driven by  $\mathcal{PT}$  symmetric nonunitary time evolution. *arXiv*, 1609.09650.
- Kitagawa, T., Berg, E., Rudner, M.S., and Demler, E. (2010). Topological characterization of periodically driven quantum systems. *Phys. Rev. B* 82, 235114.
- Kunst, F.K., Edvardsson, E., Budich, J.C., and Bergholtz, E.J. (2018). Biorthogonal bulk-boundary correspondence in non-Hermitian systems. *Phys. Rev. Lett.* 121, 026808.
- Lee, C.H., and Thomale, R. (2019). Anatomy of skin modes and topology in non-Hermitian systems. *Phys. Rev. B* 99, 201103.
- Lee, T.E. (2016). Anomalous edge state in a non-Hermitian lattice. *Phys. Rev. Lett.* 116, 133903.
- Li, J., Harter, A.K., Liu, Ji, de Melo, L., Joglekar, Y.N., and Luo, L. (2019). Observation of parity-time symmetry breaking transitions in a dissipative floquet system of ultracold atoms. *Nat. Commun.* 10, 855.
- Liang, S.-D., and Huang, G.-Y. (2013). Topological invariance and global Berry phase in non-Hermitian systems. *Phys. Rev. A* 87, 012118.
- Lieu, S. (2018). Topological phases in the non-Hermitian Su-Schrieffer-Heeger model. *Phys. Rev. B* 97, 045106.
- Martinez Alvarez, V.M., Barrios Vargas, J.E., and Foa Torres, L.E.F. (2018). Non-Hermitian robust edge states in one dimension: anomalous localization and eigenspace condensation at exceptional points. *Phys. Rev. B* 97, 121401.
- Moessner, R., and Sondhi, S.L. (2017). Equilibration and order in quantum Floquet matter. *Nat. Phys.* 13, 424.
- Özdemir, S.K., Rotter, S., Nori, F., and Yang, L. (2019). Parity-time symmetry and exceptional points in photonics. *Nat. Mater.* 18, 783–798.
- Poli, C., Bellec, M., Kuhl, U., Mortessagne, F., and Schomerus, H. (2015). Selective enhancement of topologically induced interface states in a dielectric resonator chain. *Nat. Commun.* 6, 6710.
- Potter, A.C., Morimoto, T., and Vishwanath, A. (2016). Classification of interacting topological Floquet phases in one dimension. *Phys. Rev. X* 6, 041001.
- Qi, X.-L., and Zhang, S.-C. (2011). Topological insulators and superconductors. *Rev. Mod. Phys.* 83, 1057.
- Rudner, M.S., Levin, M., and Levitov, L.S. (2016). Survival, decay, and topological protection in non-Hermitian quantum transport. *arXiv*, 1605.07652.
- Rudner, M.S., and Levitov, L.S. (2009). Topological transition in a non-Hermitian quantum walk. *Phys. Rev. Lett.* 102, 065703.
- Rudner, M.S., Lindner, N.H., Berg, E., and Levin, M. (2013). Anomalous edge states and the bulk-edge correspondence for periodically driven two-dimensional systems. *Phys. Rev. X* 3, 031005.
- Schomerus, H. (2013). Topologically protected midgap states in complex photonic lattices. *Opt. Lett.* 38, 1912–1914.
- Skyrme, T.H.R. (1962). A unified field theory of mesons and baryons. *Nucl. Phys.* 31, 556–569.
- Song, B., Zhang, L., He, C., Poon, T.F.J., Hajiyev, E., Zhang, S., Liu, X.-J., and Jo, G.-B. (2018). Observation of symmetry-protected topological band with ultracold fermions. *Sci. Adv.* 4, eaao4748.
- Su, W.-P., Schrieffer, J.R., and Heeger, A.J. (1979). Solitons in polyacetylene. *Phys. Rev. Lett.* 42, 1698.
- Tarnowski, M., Ünal, F.N., Fläschner, N., S Rem, B., Eckardt, A., Sengstock, K., and Weitenberg, C. (2019). Measuring topology from dynamics by obtaining the Chern number from a linking number. *Nat. Commun.* 10, 1728.
- Titum, P., Berg, E., Rudner, M.S., Refael, G., and Lindner, N.H. (2016). Anomalous Floquet-Anderson insulator as a nonadiabatic quantized charge pump. *Phys. Rev. X* 6, 021013.
- Vajna, S., and Dóra, B. (2015). Topological classification of dynamical phase transitions. *Phys. Rev. B* 91, 155127.
- Wang, C., Zhang, P., Chen, X., Yu, J., and Zhai, H. (2017). Scheme to measure the topological number of a Chern insulator from quench dynamics. *Phys. Rev. Lett.* 118, 185701.
- Wang, K., Qiu, X., Xiao, L., Zhan, X., Bian, Z., Sanders, B.C., Yi, W., and Xue, P. (2019a). Observation of emergent momentum-time skyrmions in parity-time-symmetric non-unitary quench dynamics. *Nat. Commun.* 10, 2293.
- Wang, K., Qiu, X., Xiao, L., Zhan, X., Bian, Z., Yi, W., and Xue, P. (2019b). Simulating dynamic quantum phase transitions in photonic quantum walks. *Phys. Rev. Lett.* 122, 020501.
- Weimann, S., Kremer, M., Plotnik, Y., Lumer, Y., Nolte, S., Makris, K.G., Segev, M., Rechtsman, M.C., and Szameit, A. (2017). Topologically protected bound states in photonic parity-time-symmetric crystals. *Nat. Mater.* 16, 433.

- Wilson, J.H., Song, J.C.W., and Refael, G. (2016). Remnant geometric Hall response in a quantum quench. *Phys. Rev. Lett.* 117, 235302.
- Xiao, L., Deng, T.-S., Wang, K., Zhu, G., Wang, Z., Yi, W., and Xue, P. (2019). Observation of non-Hermitian bulk-boundary correspondence in quantum dynamics. arXiv, 1907.12566.
- Xiao, L., Zhan, X., Bian, Z.H., Wang, K., Zhang, X., Wang, X.P., Li, J., Mochizuki, K., Kim, D., Kawakami, N., et al. (2017). Observation of topological edge states in parity-time-symmetric quantum walks. *Nat. Phys.* 13, 1117–1123.
- Yang, C., Li, L., and Chen, S. (2018). Dynamical topological invariant after a quantum quench. *Phys. Rev. B* 97, 060304.
- Yao, S., Song, F., and Wang, Z. (2018). Non-Hermitian Chern bands. *Phys. Rev. Lett.* 121, 136802.
- Yao, S., and Wang, Z. (2018). Edge states and topological invariants of non-Hermitian systems. *Phys. Rev. Lett.* 121, 086803.
- Yokomizo, K., and Murakami, S. (2019). Non-bloch band theory of non-Hermitian systems. *Phys. Rev. Lett.* 123, 066404.
- Zeuner, J.M., Rechtsman, M.C., Plotnik, Y., Lumer, Y., Nolte, S., Rudner, M.S., Segev, M., and Szameit, A. (2015). Observation of a topological transition in the bulk of a non-Hermitian system. *Phys. Rev. Lett.* 115, 040402.
- Zhan, X., Xiao, L., Bian, Z., Wang, K., Qiu, X., Sanders, B.C., Yi, W., and Xue, P. (2017). Detecting topological invariants in nonunitary discrete-time quantum walks. *Phys. Rev. Lett.* 119, 130501.
- Zhang, L., Zhang, L., and Liu, X.-J. (2019). Dynamical detection of topological charges. *Phys. Rev. A* 99, 053606.
- Zhang, L., Zhang, L., Niu, S., and Liu, X.-J. (2018). Dynamical classification of topological quantum phases. *Sci. Bull.* 63, 1385–1391.
- Zhou, L., Wang, Q.-H., Wang, H., and Gong, J. (2018). Dynamical quantum phase transitions in non-Hermitian lattices. *Phys. Rev. A* 98, 022129.
- Zhu, B., Lü, R., and Chen, S. (2014). Pt symmetry in the non-Hermitian Su-Schrieffer-Heeger model with complex boundary potentials. *Phys. Rev. A* 89, 062102.

**Supplemental Information**

**Fixed Points and Dynamic Topological Phenomena  
in a Parity-Time-Symmetric Quantum Quench**

**Xingze Qiu, Tian-Shu Deng, Ying Hu, Peng Xue, and Wei Yi**

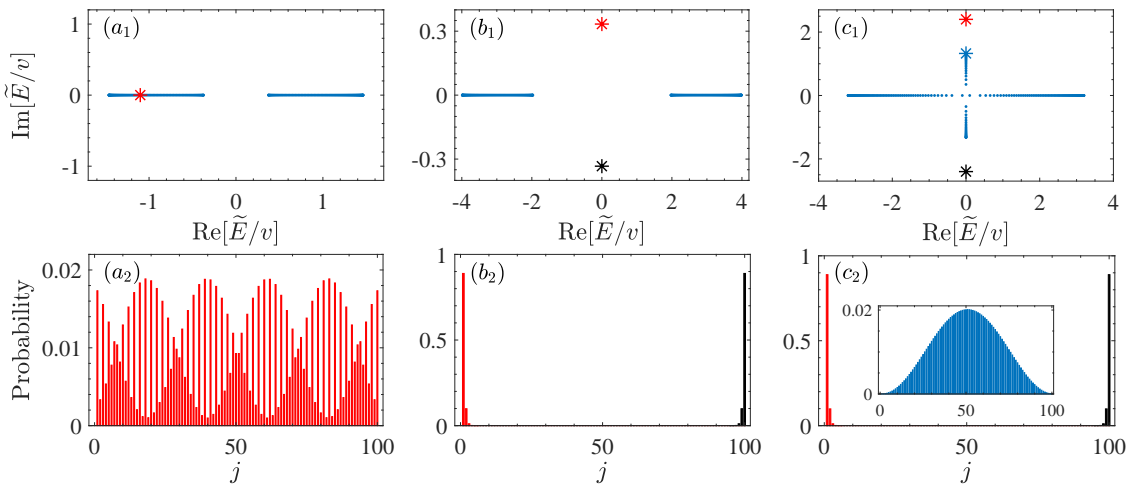


**FIG. S1 Eigenspectra and eigen wavefunctions for non-Hermitian SSH models with open boundary conditions.** We numerically diagonalize the Hamiltonian (1) with open boundary conditions on a lattice with  $L = 100$  sites. Eigenspectra are shown in the first row, and eigen wave functions corresponding to states marked by asterisks are shown in the second row. The parameters are: (a1)(a2) ( $u = 1/3v, w = 1/2v$ ) and  $\nu = 0$ ; (b1)(b2) ( $u = 1/3v, w = 3v$ ) and  $\nu = 1$ ; (c1)(c2) ( $u = 2.4v, w = 3v$ ) and  $\nu = 1$ . (c1)(c2) are in the  $\mathcal{PT}$ -symmetry-broken regime. While a typical  $\mathcal{PT}$ -symmetry-preserving bulk state with an extended wave function is shown in (a2), topological edge states localized at two ends of the lattice emerge in both the  $\mathcal{PT}$ -symmetry-preserving regime (b1)(b2) and the  $\mathcal{PT}$ -symmetry-broken regime (c1)(c2), where  $\nu = 1$ . Note that  $\mathcal{PT}$ -symmetry-broken bulk states with imaginary eigenenergies are present in the  $\mathcal{PT}$ -symmetry-broken regime (c1)(c2), but their spatial wave functions are extended rather than localized, as illustrated in the inset of (c2). Related to Fig. 1(b).

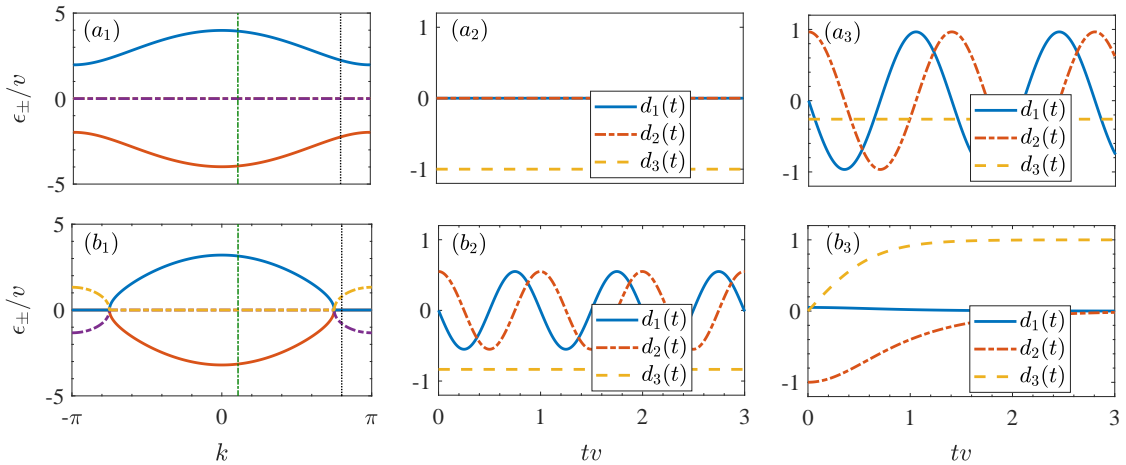


**FIG. S2 Dynamics of spin textures  $d(k, t)$  under different parameters.** (a1) Eigenenergy spectra for  $H_a^f$  characterized by  $(u^f = v/3, v^f = v, w^f = 3v)$ . (a2)(a3) Time evolution of  $d(k, t)$  at fixed momenta as the system is quenched into  $H_a^f$ . (b1) Eigenenergy spectra for  $H_b^f$  characterized by  $(u^f = 2.4v, v^f = v, w^f = 3v)$ . (b2)(b3) Time evolution of  $d(k, t)$  at fixed momenta as the system is quenched into  $H_b^f$ . For the time evolution, the momenta are taken at the fixed point  $k \approx 0.34$  in (a2)(b2), and at  $k = 4\pi/5$  in (a3)(b3), as indicated by the vertical green and black lines in (a1)(b1). In all quench processes, the initial state in each  $k$ -sector is the eigenstate  $|\psi_-^i\rangle$  of the initial Hamiltonian  $H_k^i$ , corresponding to  $(u^i = v/3, v^i = v, w^i = v/2)$ . Related to Fig. 2.

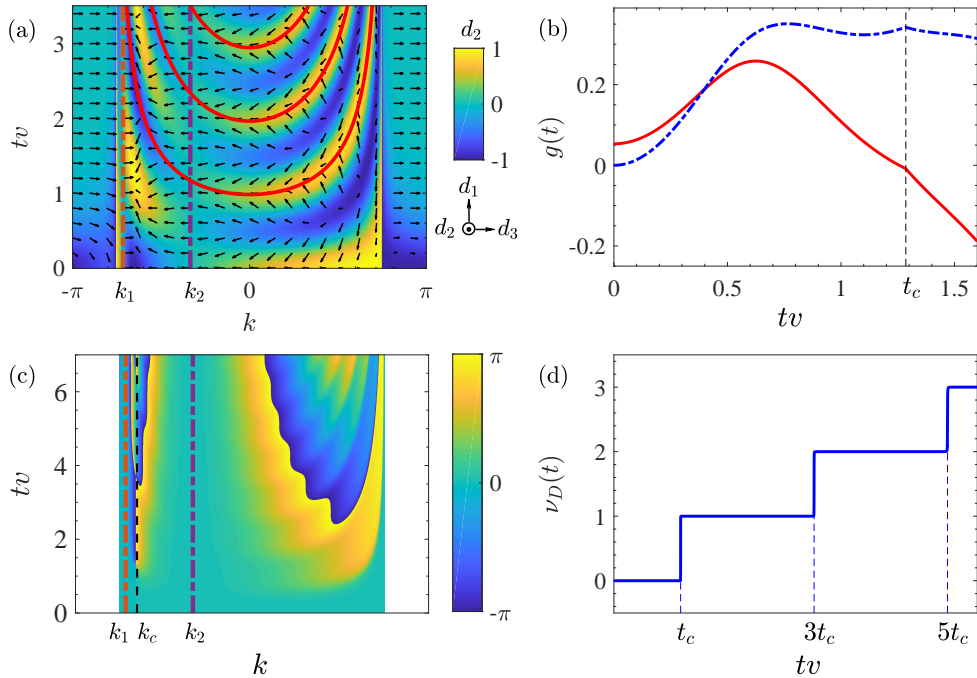


**FIG. S3 Coincidental topological phenomena when the final Hamiltonian is in the  $\mathcal{PT}$ -symmetry-broken regime.** The initial Hamiltonian is characterized by ( $u^i = v/3, v^i = v, w^i = v/2$ ), and the final Hamiltonian is characterized by ( $u^f = 2.4v, v^f = v, w^f = 3v$ ). (a) Spin texture  $d(k,t)$  in the  $k$ - $t$  plane. (b) Rate function  $g(t)$  of the quench process (red solid), where contribution from all momenta in 1BZ are considered. For comparison, we also plot the rate function where only Loschmidt amplitude in the momentum range with real  $E_k^f$  are considered (blue dashed). The signal for DQPT is more apparent in the latter. (c) PGP in the momentum range with real  $E_k^f$ . Note that PGP in the momentum range with imaginary  $E_k^f$  is not well-defined. (d)  $\nu_D$  as integrated between the fixed points, where  $t_c = \pi/E_{k_c}^f$ . Related to Figs. 3 and 4.

## Transparent Methods

### I. Topological invariant through the global Berry phase

Topological invariants defined through the global Berry phase  $\varphi_B$  have the advantage that they invoke the formalism of biorthonormal basis and characterize topological properties in both the  $\mathcal{PT}$ -symmetry-preserving and broken regimes. The resulting winding number  $\nu = \varphi_B/2\pi$  has a geometric interpretation, i.e., the number of times the unit vector  $\mathbf{n} = \frac{1}{\sqrt{h_1^2+h_2^2}}(h_1, h_2, 0)$ , which lies in the  $x$ - $y$  plane, winds around the  $z$ -axis as  $k$  varies through the 1BZ. Here,  $\{x, y, z\}$  corresponds to the indices  $\{1, 2, 3\}$ , respectively. This geometric interpretation thus makes connection with previously defined generalized winding numbers in non-Hermitian settings (Rudner et al., 2016; Zeuner et al., 2015; Zhan et al., 2017). It also reduces to the generalized Zak phase for  $\mathcal{PT}$ -symmetric non-Hermitian systems in the  $\mathcal{PT}$ -symmetry-preserving regime (Kim et al., 2016; Xiao et al., 2017).

To explicitly demonstrate that the winding number defined through the global Berry phase serves as the topological invariant of the system, we numerically calculate the eigenspectra  $\tilde{E}$  of Hamiltonian (1) in various regimes under open boundary conditions. As illustrated in Fig. S1, localized topological edge states with  $\text{Re}(\tilde{E}) = 0$  emerge in both  $\mathcal{PT}$ -symmetry-preserving and broken regimes, so long as  $\nu = 1$ . In the  $\mathcal{PT}$ -symmetry-broken case, bulk states with  $\text{Re}(\tilde{E}) = 0$  also exist, but their wave functions are extended and the imaginary parts of their eigenenergies are smaller than that of the edge state.

As is clear from Fig. S1, all bulk eigenstates are extended. The non-Hermitian skin effect (Kunst et al., 2018; Lee, 2016; Yao et al., 2018; Yao and Wang, 2018) is therefore absent from our model under an open-boundary condition, and the bulk winding number calculated through the global Berry phase is sufficient in correctly predicting the existence and number of topological edge states.

### II. Evolution of the density matrix

The time-dependent density matrix in the  $k$ -sector is written as

$$\rho(k, t) = \frac{1}{2} [\tau_0 + \mathbf{d}(k, t) \cdot \boldsymbol{\tau}]. \quad (\text{S1})$$

When  $E_k^f$  is real, we have

$$d_0 = c_+^* c_+ + c_-^* c_-, \quad (\text{S2})$$

$$d_1 = (c_-^* c_+ e^{-i2E_k^f t} + \text{c.c.})/d_0, \quad (\text{S3})$$

$$d_2 = i(c_-^* c_+ e^{-i2E_k^f t} - \text{c.c.})/d_0, \quad (\text{S4})$$

$$d_3 = (c_+^* c_+ - c_-^* c_-)/d_0, \quad (\text{S5})$$

where  $c_\mu = \langle \chi_\mu^f | \psi_-^i \rangle$  as defined in the main text. Apparently, while  $\mathbf{d}(k, t)$  is a real unit vector,  $d_3$  is time independent, and both  $d_1$  and  $d_2$  are oscillatory in time with a momentum-dependent period  $t_0 = \pi/E_k^f$ . The fixed-point condition is satisfied when  $c_- = 0$  or  $c_+ = 0$ , as  $d_1 = d_2 = 0$  and  $|d_3| = 1$ . We further parameterize  $\mathbf{d}(k, t)$  as follows

$$d_1(\theta, \varphi) = \sin \theta \cos(\varphi + \delta\varphi), \quad (\text{S6})$$

$$d_2(\theta, \varphi) = \sin \theta \sin(\varphi + \delta\varphi), \quad (\text{S7})$$

$$d_3(\theta) = \cos \theta, \quad (\text{S8})$$

where the parameters  $(\theta, \varphi, \delta\varphi)$  are defined through

$$c_+ = \sqrt{d_0} e^{i\varphi_+} \cos \frac{\theta}{2}, \quad (\text{S9})$$

$$c_- = \sqrt{d_0} e^{i\varphi_-} \sin \frac{\theta}{2}, \quad (\text{S10})$$

$$\varphi = 2E_k^f t, \quad (\text{S11})$$

$$\delta\varphi = \varphi_- - \varphi_+. \quad (\text{S12})$$

Here,  $\theta \in [0, \pi]$ ,  $\varphi \in [0, 2\pi]$ , and  $\delta\varphi$  is a constant.  $\mathbf{d}(k, t)$  therefore depicts a vector evolving on the Bloch sphere characterized by  $(\theta, \varphi)$ , as illustrated in Fig. 2(a) of the main text. We identify  $\mathbf{d}(k, t)$  associated with the fixed point  $c_- = 0$  ( $c_+ = 0$ ) as the north (south) pole of the Bloch sphere. Hence, when  $|c_-| = |c_+|$ ,  $d_3 = 0$  and the corresponding  $\mathbf{d}(k, t)$  lies on the equator of the Bloch sphere.

When  $E_k^f$  is imaginary, we have

$$d_0 = c_+^* c_+ e^{-i2E_k^f t} + c_-^* c_- e^{i2E_k^f t}, \quad (\text{S13})$$

$$d_1 = (c_-^* c_+ + \text{c.c.})/d_0, \quad (\text{S14})$$

$$d_2 = i(c_-^* c_+ - \text{c.c.})/d_0, \quad (\text{S15})$$

$$d_3 = (c_+^* c_+ e^{-i2E_k^f t} - c_-^* c_- e^{i2E_k^f t})/d_0. \quad (\text{S16})$$

Without loss of generality, we have assume  $\text{Im}(E_k^f) > 0$ . We parameterize  $\mathbf{d}(k, t)$  as

$$d_1(\theta, \varphi) = \sin \theta \cos \varphi, \quad (\text{S17})$$

$$d_2(\theta, \varphi) = \sin \theta \sin \varphi, \quad (\text{S18})$$

$$d_3(\theta, \varphi) = \cos \theta, \quad (\text{S19})$$

where the parameters  $(\theta, \varphi)$  are defined through

$$c_+ = \sqrt{d_0} e^{iE_k^f t} e^{i\varphi_+} \cos \frac{\theta}{2}, \quad (\text{S20})$$

$$c_- = \sqrt{d_0} e^{-iE_k^f t} e^{i\varphi_-} \sin \frac{\theta}{2}, \quad (\text{S21})$$

$$\varphi = \varphi_- - \varphi_+. \quad (\text{S22})$$

Here,  $\theta \in [0, \pi]$ ,  $\varphi \in [0, 2\pi)$ . In this case,  $\mathbf{d}(k, t)$  is still a real unit vector on a Bloch sphere characterized by  $(\theta, \varphi)$ . As we show in the next section, one can prove  $|c_+| \equiv |c_-|$  in this case. Therefore, we have  $d_3(k, t=0) = 0$ ,

$\lim_{t \rightarrow \infty} d_3(k, t) = 1$ , and  $\lim_{t \rightarrow \infty} d_1(k, t) = \lim_{t \rightarrow \infty} d_2(k, t) = 0$ . The vector  $\mathbf{d}(k, t)$  thus necessarily lies on the equator of the Bloch sphere at  $t = 0$  and approaches the north pole in the long-time limit, as illustrated in Fig. 2(b) of the main text. The density matrix in the corresponding  $k$ -sector approaches a steady-state value in the long-time limit, and fixed points do not exist.

In Fig. S2, we demonstrate typical time evolutions of  $\mathbf{d}(k, t)$  at different momenta, as the system is quenched from an initial Hamiltonian in the  $\mathcal{PT}$ -symmetry-preserving regime to final Hamiltonians in either the  $\mathcal{PT}$ -symmetry-preserving regime or the symmetry-broken regime, respectively. At fixed points [Fig. S2(a2)],  $\mathbf{d}(k, t)$  is time independent. At momenta with real  $E_k^f$  [Fig. S2(a3)(b2)],  $\mathbf{d}(k, t)$  is oscillatory, regardless of whether the final Hamiltonian is  $\mathcal{PT}$ -symmetry-preserving or not. At momenta with imaginary  $E_k^f$  when the final Hamiltonian is in the  $\mathcal{PT}$ -symmetry-broken regime [Fig. S2(b3)],  $\mathbf{d}(k, t)$  approaches a steady-state value in the long-time limit.

### III. Existence of fixed points

In this section, we show that the existence and number of fixed points are intimately connected with the generalized winding numbers of  $H^i$  and  $H^f$ , when both Hamiltonians belong to the  $\mathcal{PT}$ -symmetry-preserving regime with completely real eigenspectra. First, we parameterize the initial state and the left eigenstate of the final Hamiltonian at momentum  $k$ , respectively, as  $|\psi_-^i\rangle = \frac{1}{\sqrt{2\cos 2\Omega^i}} \left( -e^{-i\Omega^i}, e^{i\phi^i} e^{i\Omega^i} \right)^T$  and  $|\chi_\pm^f\rangle = \frac{1}{\sqrt{2\cos 2\Omega^f}} \left( \pm e^{\pm i\Omega^f}, e^{-i\phi^f} e^{\mp i\Omega^f} \right)$ . Here,  $\sin 2\Omega^\beta = u^\beta/h^\beta$  ( $\beta = i, f$ ),  $h^\beta e^{i\phi^\beta} = h_1^\beta + ih_2^\beta$ , where components of  $\mathbf{h}^i$  and  $\mathbf{h}^f$  are associated with  $H_k^i$  and  $H_k^f$ , respectively. Note that  $\Omega^\beta$  is real when  $E_k^\beta$  is real. Importantly,  $\phi^\beta$  is the polar angle of the vector  $\mathbf{h}^\beta$ , which is associated with the generalized winding number  $\nu^\beta$  of the Hamiltonian  $H^\beta$  through  $\nu^\beta = \oint dk \partial\phi^\beta / \partial k$  ( $k \in 1BZ$ ).

We then have

$$c_\pm = \frac{\mp e^{-i(\Omega^i \mp \Omega^f)} + e^{i\phi^0} e^{i(\Omega^i \mp \Omega^f)}}{2\sqrt{\cos 2\Omega^i \cos 2\Omega^f}}, \quad (\text{S23})$$

where  $\phi^0 = \phi^i - \phi^f$ . Consider a unit vector  $\mathbf{n}^0$  on the  $x$ - $y$  plane whose polar angle is given by  $\phi^0$ . As  $k \in 1BZ$ , the number of times  $\mathbf{n}^0$  winds around the  $z$ -axis is therefore  $\oint dk \partial\phi^0 / \partial k = \nu^i - \nu^f$ . From Eq. (S23), the condition for  $c_\pm = 0$  is  $\phi^0 = 2(\Omega^f - \Omega^i) \pmod{2\pi}$  and  $\phi^0 = \pi - 2(\Omega^f + \Omega^i) \pmod{2\pi}$ , respectively. Therefore, the number of fixed points with  $c_+ = 0$  or  $c_- = 0$  should be at least  $|\nu^i - \nu^f|$  each.

Conversely, when  $H^f$  is in the  $\mathcal{PT}$ -symmetry-broken regime, the corresponding  $E_k^f$  becomes imaginary for a certain range of  $k$ . At these momenta,  $\Omega^f$  becomes complex, which invalidates the argument following Eq. (S23). Further, we have

$$|c_\pm(k)|^2 = \frac{\cosh 2\omega_k^f - \sin(\phi_k^0 + 2\Omega_k^i)}{2\cos 2\Omega_k^i \sinh 2\omega_k^f}, \quad (\text{S24})$$

where  $\omega_k^f = \text{Im}(\Omega_k^f)$ . Hence  $|c_+(k)| \equiv |c_-(k)|$  in this case. Note that  $c_\pm$  cannot vanish simultaneously at the same  $k$ , as otherwise  $|\psi_-^i(k)\rangle = \sum_\mu c_\mu(k) |\psi_\mu^f(k)\rangle = 0$ .

When the system is quenched between different topological phases in the  $\mathcal{PT}$ -symmetry-preserving regime, fixed points with  $c_+ = 0$  and those with  $c_- = 0$  always emerge in pairs. As we have discussed in the main text, this gives rise to dynamic Chern numbers and dynamic skyrmions in the momentum-time space. As  $|c_+| - |c_-|$  is a continuous function of  $k$ , there must be at least one critical momentum satisfying  $|c_+(k_c)| = |c_-(k_c)|$  inbetween two fixed points of different kinds. We thus conclude that DQPTs also occur in this case.

### IV. Dynamic Chern number

Between two arbitrary fixed points  $k_m$  and  $k_n$ , the dynamic Chern number is defined as

$$C_{mn} = \frac{1}{4\pi} \int_{k_m}^{k_n} dk \int_0^{t_0} dt [\mathbf{d}(k, t) \times \partial_t \mathbf{d}(k, t)] \cdot \partial_k \mathbf{d}(k, t). \quad (\text{S25})$$

The Chern number is well-defined so long as  $E_k^f$  is real in the momentum submanifold spanned by  $k_m$  and  $k_n$ .

Following the parameterization of  $\mathbf{d}(k, t)$  in Eqs. (S6-S8), we have  $[\mathbf{d}(\theta, \varphi) \times \partial_\varphi \mathbf{d}(\theta, \varphi)] \cdot \partial_\theta \mathbf{d}(\theta, \varphi) = -\sin \theta$ . This allows us to evaluate the dynamic Chern number between two adjacent fixed poits  $k_m$  and  $k_{m+1}$  in the following cases:

**A.**  $c_+(k_{m+1}) = 0$  and  $c_-(k_m) = 0$

As there are no other fixed points inbetween  $k_m$  and  $k_{m+1}$ ,  $\theta$  should be integrated in the range  $[0, \pi]$ . We have

$$C_{m,m+1} = \frac{1}{4\pi} \int_0^\pi d\theta \int_0^{2\pi} d\varphi [\mathbf{d}(\theta, \varphi) \times \partial_\varphi \mathbf{d}(\theta, \varphi)] \cdot \partial_\theta \mathbf{d}(\theta, \varphi) = \frac{1}{4\pi} \int_0^\pi d\theta \int_0^{2\pi} d\varphi (-\sin \theta) = -1. \quad (\text{S26})$$

### B. $c_+(k_m) = 0$ and $c_-(k_{m+1}) = 0$

Similarly, we have

$$C_{m,m+1} = \frac{1}{4\pi} \int_\pi^0 d\theta \int_0^{2\pi} d\varphi [\mathbf{d}(\theta, \varphi) \times \partial_\varphi \mathbf{d}(\theta, \varphi)] \cdot \partial_\theta \mathbf{d}(\theta, \varphi) = -\frac{1}{4\pi} \int_0^\pi d\theta \int_0^{2\pi} d\varphi (-\sin \theta) = 1. \quad (\text{S27})$$

### C. $c_+(k_m) = 0$ and $c_+(k_{m+1}) = 0$ , or $c_-(k_m) = 0$ and $c_-(k_{m+1}) = 0$

In this case,  $\theta$  is integrated from 0 to 0 or from  $\pi$  to  $\pi$ , therefore  $C_{m,m+1} = 0$ .

For arbitrary fixed points  $k_m$  and  $k_n$ , by successively applying the results above between adjacent fixed points, we have:  $C_{mn} = 1$  when  $c_+(k_m) = 0$  and  $c_-(k_n) = 0$ ;  $C_{mn} = -1$  when  $c_-(k_m) = 0$  and  $c_+(k_n) = 0$ ; when the two fixed points are of the same kind,  $C_{mn}$  vanishes.

## V. Coincidental fixed points and topological phenomena in the $\mathcal{PT}$ -symmetry-broken regime

As we have seen in Fig. S2(b1), momentum regime with real  $E_k$  exists even when the overall Hamiltonian  $H = \sum_{k \in 1\text{BZ}} H_k$  is in the  $\mathcal{PT}$ -symmetry-broken regime. Hence, coincidental fixed points can still exist when  $H^f$  is in the  $\mathcal{PT}$ -symmetry-broken regime, provided that  $E_k^f$  is real at these fixed points and that the initial and final Hamiltonians belong to different topological phases.

As an example, in Fig. S3, we illustrate the emergence of coincidental dynamic topological phenomena when  $H^f$  is in the  $\mathcal{PT}$ -symmetry-broken regime. As indicated by vertical dashed lines in Fig. S3(a), two fixed points exist at  $k_1 \approx -2.25$ ,  $k_2 \approx -1.05$ . As both  $E_{k_1}^f$  and  $E_{k_2}^f$  are real, dynamic Chern number is well-defined in the  $S^2$  manifold spanned by  $(k_1, k_2)$  in momentum space and  $(0, t_0)$  in temporal space.

On the other hand, the existence of coincidental fixed points in the  $\mathcal{PT}$ -symmetry-broken regime still gives rise to critical point  $k_c \approx -2.05$  in momentum space, where the  $\phi_k^G(t)$  undergo abrupt changes. Correspondingly, periodic nonanalyticities exist in  $g(t)$ . However, as illustrated in Fig. S3(b), the signals for DQPT get drowned out by contributions from the momentum-range with imaginary eigenenergies, whose signals get exponentially enhanced over time. In this case, quantized dynamic topological order parameter  $\nu_D$  can be defined and calculated [see Fig. S3(d)] in the momentum submanifold spanned by  $k_1$  and  $k_2$ , with  $\nu_D(t) = \frac{1}{2\pi} \int_{k_1}^{k_2} \frac{\partial \phi_k^G(t)}{\partial k} dk$ .

## References

- D. Kim, M. Ken, N. Kawakami, and H. Obuse (2016), “Floquet topological phases driven by  $\mathcal{PT}$  symmetric nonunitary time evolution,” Preprint arXiv:1609.09650 .
- F. K. Kunst, E. Edvardsson, J. C. Budich, and E. J. Bergholtz (2018), “Biorthogonal bulk-boundary correspondence in non-Hermitian systems,” Phys. Rev. Lett. **121** (2), 026808.
- T. E Lee (2016), “Anomalous edge state in a non-hermitian lattice,” Phys. Rev. Lett. **116** (13), 133903.
- M. S. Rudner, M. Levin, and L. S. Levitov (2016), “Survival, decay, and topological protection in non-Hermitian quantum transport,” Preprint arXiv:1605.07652 .
- L. Xiao, X. Zhan, Z. H. Bian, K. Wang, X. Zhang, X. P. Wang, J. Li, K. Mochizuki, D. Kim, N. Kawakami, W. Yi, H. Obuse, B. C. Sanders, and P. Xue (2017), “Observation of topological edge states in parity-time-symmetric quantum walks,” Nat. Phys. **13** (11), 1117.
- S. Yao, F. Song, and Z. Wang (2018), “Non-hermitian chern bands,” Phys. Rev. Lett. **121** (13), 136802.
- S. Yao, and Z. Wang (2018), “Edge states and topological invariants of non-Hermitian systems,” Phys. Rev. Lett. **121** (8), 086803.
- J. M. Zeuner, M. C. Rechtsman, Y. Plotnik, Y. Lumer, S. Nolte, M. S. Rudner, M. Segev, and A. Szameit (2015), “Observation of a topological transition in the bulk of a non-Hermitian system,” Phys. Rev. Lett. **115** (4), 040402.
- X. Zhan, L. Xiao, Z. Bian, K. Wang, X. Qiu, B. C. Sanders, W. Yi, and P. Xue (2017), “Detecting topological invariants in nonunitary discrete-time quantum walks,” Phys. Rev. Lett. **119** (13), 130501.